

# Enhanced angular overlap model for f-electron non-metallic systems

Z. Gajek\*

*Institute of Low Temperature and Structure Research,  
Polish Academy of Sciences, P Nr 1410, 50-950 Wrocław 2, Poland*

(Dated: May 12, 2017)

An efficient method of interpretation of the crystal field effect in non-metallic f-electron systems, the *enhanced angular overlap model* (EAOM), is presented. The method is established on the ground of perturbation expansion of the effective Hamiltonian for localized electrons and first principles calculations related to available experimental data. Series of actinide compounds,  $AnO_2$ , oxychalcogenides,  $AnOX$  and dichalcogenides  $UX_2$  where  $X = S, Se, Te$  and  $An = U, Np$  serve as a probe of effectiveness of the proposed method. An idea is to enhance the usual angular overlap model with *ab initio* calculations of those contributions to the crystal field potential, which cannot be represented by the usual angular overlap model (AOM). The enhancement leads to an improved fitting and makes the approach intrinsically coherent. In addition, the *ab initio* calculations of the main, AOM-consistent part of the crystal field potential allows one to fix the material-specific relations for the EAOM parameters in the effective Hamiltonian. In consequence, the electronic structure interpretation based on EAOM can be extended to the systems of the lowest point symmetries or/and deficient experimental data. Several examples illustrating the promising capabilities of EAOM are given.

PACS numbers: 71.23.An 71.70.Ch 75.30.Gw

## I. INTRODUCTION

A list of phenomena traditionally discussed in the context of the crystal field (CF) like optical excitations, Schottky effect, Van Vleck susceptibility etc has been extended in last decades to include so intriguing and different manifestations of many-body effects as unconventional superconductivity, Kondo-like behavior, magnetic rearrangements or non-Fermi liquid. Complexity of these phenomena contrasts with apparent simplicity the one-electron, local CF potential in the effective Hamiltonian. Nevertheless, its reliable determination meets serious difficulties even today, 75 years after Bethe considered the CF effect for the first time.<sup>1</sup> These concern not only calculations from first principles but also common phenomenological schemes based exclusively on the symmetry arguments. In practice, only compounds of the highest symmetries can be handled satisfactorily. In most cases, the usual least squares fitting of all the parameters in the effective Hamiltonian requires additional, more or less heuristic reasoning referring to physical or chemical foundations. Alternatively, simplified phenomenological models are employed to circumvent the problem of over-numerous parameters. Accuracy of these models is one of the issues the present discussion addresses. We focus on the angular overlap model (AOM) inspired by the molecular orbital theory<sup>2,3</sup> and confirmed by further theoretical calculations.<sup>4,5</sup> AOM assumes, similarly as the superposition model (SPM)<sup>6</sup>, the total CF potential in the form of superposition of axial potentials due to ligands represented by a set of intrinsic parameters. The number of free parameters is remarkably reduced in comparison with the basal parametrization, especially for low-symmetry systems but the approximations are rather crude. A more refined analysis of the experimental data,

having fundamental meaning for subtle magnetic properties or cooperative phenomena at low temperatures, may require more rigorous methods. Can these simplified CF models be improved without increasing the number of free parameters? This question is discussed here on the grounds of *ab initio* calculations for a series of actinide compounds.

There are two general ways to determine the CF potential from first principles: one based on the perturbation theory and the idea of the effective Hamiltonian for localized, open shell electrons<sup>4</sup> and second developed on the grounds of the density functional theory (DFT).<sup>7,8</sup> Taking into account proximity of the band states or/and widening of the localized  $nf$  states, DFT seems to be more suitable method for metallic systems. However, the early implementations of DFT based on the local spin density approximation (LSDA) had failed to predict not only the subtle magnetic, low temperature thermodynamic properties and the low energy spectra but even some of the main characteristics of the crystals. For instance, antiferromagnetic semiconductor  $UO_2$  becomes a ferromagnetic metal.<sup>9</sup> Over the years some inherent shortcomings of LSDA, like double counting of states or requirement for the electron density to be a slowly varying function, were lessened or removed by various corrections: generalized gradient approximation, U approximation, self-interaction correction or, more recently, the hybrid density-functional theory.<sup>9</sup> Nevertheless, these improvements, to our best knowledge, have not eliminated completely the problems related to the CF effect (see discussion in Ref. 10, p. 206).

An alternative approach,<sup>10,11</sup> based on the perturbation expansion of the effective Hamiltonian seems to be more efficient and reliable in providing material-specific details of the electronic structure. The model was developed for non-metallic systems successively by Sugano

and Schulman,<sup>12</sup> Newman and coworkers,<sup>6,13</sup> Faucher and Garcia,<sup>14</sup> and others. (see Refs. 10,13 and references therein) The effective CF potential appears in this approach as a sum of several contributions, most of which obey the assumptions of the mentioned simplified phenomenological models.

In metallic systems, additional mechanisms, apart from those characteristic for insulating crystals, have to be considered:<sup>10</sup> mixing of the localized and band states (hybridization), static and dynamic screening of the conduction electrons including an offset screening of the carriers occupying a virtual bond state. None of them can be regarded as a pure superposition of the nearest neighbor contributions. Moreover, the role of each mechanism remains unclear; for instance, the hybridization term alone can represent almost the whole CF effect for some compounds,<sup>15</sup> but for others it is only one of the important contributions.<sup>16</sup> In addition, the dynamic correlations become increasingly important as the localized state nears the conduction band giving rise to the many-electron crystal field effects or even leading to a breakdown of the effective Hamiltonian theory for localized electrons. Thus, an extension of the crystal field theory towards self-consistent models for mixed systems of localized and itinerant electrons attracts growing attention recently.<sup>17</sup> However, material-specific results based on these efforts has not been achieved yet and we have to confine discussion to simpler systems in which an admixture of the band states to the localized ones or a mixing of the states localized on adjacent atoms can be treated as an additional perturbation term in our effective Hamiltonian. We can only notice that there exists a subgroup of metallic systems for which the basic CF mechanisms remain essentially the same as those for ionic crystals.<sup>18</sup>

Accuracy of the simplified models has been discussed on the grounds of numerical simulations for actinide compounds.<sup>5</sup> It has turned out that the lattice contributions were not always negligible and the  $e_\delta$  contribution (see section II B) has not behaved as a characteristic, intrinsic parameter of the metal-ligand ( $ML$ ) interaction. Moreover, the present paper shows that the main AOM energies,  $e_\sigma$  and  $e_\pi$ , may also fail a more rigorous test of their transferability. Thus we propose a quasi-phenomenological approach that links the simplified phenomenological model with partial *ab initio* calculations: the *enhanced angular overlap model* (EAOM).

The paper is organized as follows: the perturbation expansion leading to the effective Hamiltonian and the angular overlap model is outlined in the section II. Details of the *ab initio* calculations, their results obtained for the first time for  $UX_2$  ( $X = S, Se, Te$ )<sup>19</sup> and those reported previously for  $AnO_2$ <sup>16</sup> and  $AnOX$ <sup>20,21</sup> are discussed in section, III including their reliability, adequacy of the superposition approximation and variation of the intrinsic parameters with distance across the series. The enhanced angular overlap model is considered in section IV together with examples of its application. Concluding remarks are provided in section V. To ensure

self-consistency of the presentation some known formulas used in the calculations are included in Appendices.

## II. FORMULATION

### A. Effective Hamiltonian

Since the theoretical model applied here has been presented elsewhere (see Ref. 10 and references therein), we only recap its main points for clarity of further discussion. The basic assumption of the model is that all magnetic electrons in a crystal occupy stationary orbitals,  $5f$  in the case of the discussed here actinide ions. The initial infinite many-electron problem is reduced then to a single cluster consisting of a metal ion and nearest neighbors - ligands. The outside of the cluster is represented by the classic electrostatic potential. The cluster itself is treated as a system of weakly interacting groups of electrons localized on different ions. This allows one to apply the group product function formalism and reduce the initial  $N$ -electron system to several subsystems of lower dimensions.<sup>4,10,22</sup> The zero-order group product wavefunctions are built up from the free-ion spin-orbitals obtained with the standard self-consistent Dirac-Slater procedure and stabilization potential wall for anions, depth of which is determined by the Madelung energy. The function basis is restricted to the ground and the most important inter- and intra-ion excited electronic configurations. Projection of the initial function space onto the ground configuration subspace, contraction of the closed shell states, and renormalization due to the nonorthogonality of the wave-functions centered on different ions are the main steps in this approach. They lead to an effective Hamiltonian defined in the restricted wave-function space spanned by the single  $5f^n$ -configuration states. The effective Hamiltonian contains several renormalization terms which can be regarded as a perturbation to the initial Hamiltonian. The theory may be easily verified by the experimental data because the same function basis is employed in the conventional phenomenological description of the electronic structure (see Appendix A). A non-spherical part of the effective Hamiltonian defines the effective CF potential  $V(\mathbf{r})$  "seen" by a  $5f$ -electron. Since all the wave-functions in our restricted function basis have the same radial part  $\frac{1}{r}P(r)$ , the Hamiltonian and all relevant operators can be contracted to the angular coordinates. The resulting operator of the CF potential  $\hat{V}(\mathbf{r}/r)$  is commonly written in a form of expansion in terms of the normalized spherical harmonics  $\hat{C}_q^{(k)}$ ,<sup>23</sup>

$$\hat{V}(\mathbf{r}/r) = \sum_{k,q} B_{kq} \hat{C}_q^{(k)}(\mathbf{r}/r), \quad (1)$$

where  $k = 2, 4, 6$  denotes rank of the spherical harmonic and  $q = -k, -k + 1, \dots, k$  runs over its components.  $B_{kq}$

are the integrals,

$$B_{kq} = \int \left[ \frac{1}{r} P_{nf}(r) \right]^2 V(\mathbf{r}) \hat{C}_q^{(k)*}(\mathbf{r}/r) d\mathbf{r}, \quad (2)$$

playing a role of adjustable CF parameters in the phenomenological theory.

### B. Angular overlap model

Angular overlap model (AOM) is a simplified phenomenological approach based on certain restrictive assumptions, inspired by the Hückel molecular orbital model.<sup>2,3</sup> From among various formulations appearing in the literature we chose one proposed by Schäffer<sup>24</sup> which does not refer to molecular orbital scheme. This formulation is consistent with the perturbation approach outlined above and the Newman superposition model<sup>6</sup> discussed later. According to it, the CF potential  $V$  is a superposition of the independent contributions - potentials  $v_t$  generated by the nearest neighbors - ligands:

$$V(\mathbf{r}) \simeq \sum_t v_t(\mathbf{r} - \mathbf{R}_t), \quad (3)$$

where  $\mathbf{R}_t$  denotes the position of the  $t$ -th ligand. Additionally, as an approximation, the local symmetry of the separated metal-ligand system is assumed to be axial.

The AOM parameter  $e_\mu^t$  of the given ligand  $t$  is defined as a matrix element of the ligand potential  $v_t$  in the coordinate system  $t$  with the  $z$  axis along the metal-ligand  $t$  linear ligator in which  $v_t$  is diagonal:

$$e_\mu^t \equiv e_\mu^t(R_t) = \langle \pm\mu | v_t | \pm\mu \rangle_t, \quad (4)$$

where the index  $\mu = 0(\sigma), 1(\pi), 2(\delta), 3(\phi)$  denotes the absolute value of the magnetic quantum number of the  $5f$ -electron. It is convenient to fix the energy scale by setting  $e_\phi = 0$ . In practice we put  $\tilde{e}_\mu \equiv e_\mu - e_\phi$  instead of  $e_\mu$ . Since only  $\tilde{e}_\mu$ 's are used hereafter, we omit the tilde for convenience. Transformation properties under the rotation group  $R_3$  of the  $l = 3$  wave-functions allow one to express the matrix elements of  $V$  in the global coordinate system in terms of  $e_\mu^t$ 's:

$$\langle m | V | m' \rangle = \sum_t \sum_\mu D_{\mu m}^{(3)*}(0, \Theta_t, \Phi_t) D_{\mu m'}^{(3)}(0, \Theta_t, \Phi_t) e_\mu^t, \quad (5)$$

where  $D_{\mu m}^{(3)}(0, \Theta_t, \Phi_t)$  is the matrix element of the irreducible representation  $D^{(3)}$  of the rotation group and  $R_t, \Theta_t, \Phi_t$  are the angular (global) coordinates of the ligand  $t$ . Eq. (5) is the fundamental equation of AOM. It relates the matrix elements of the CF potential to the intrinsic parameters describing the individual metal-ligand pairs through rotation matrices dependent on the geometry of the coordination polyhedron.

For practical purposes it is advisable to relate the AOM parameters to the basic CF parameters  $B_{kq}$ . Comparing

the right side of Eq. (5) with the matrix elements of the potential given by the expansion (1) and using the properties of tensor operators and the rotation matrices<sup>25,26</sup> we obtain after some manipulation the following relation:

$$B_{kq} = \sum_\mu W_{kq}^\mu e_\mu \quad (6)$$

where

$$W_{kq}^\mu = \frac{2k+1}{7} \left[ \begin{pmatrix} 3 & k & 3 \\ 0 & 0 & 0 \end{pmatrix} \right]^{-1} (-1)^\mu (2 - \delta_{\mu 0}) \times \\ \times \begin{pmatrix} 3 & k & 3 \\ -\mu & 0 & \mu \end{pmatrix} \sum_t C_q^{(k)*}(\Theta_t, \Phi_t) s_\mu^t \quad (7)$$

$$s_\mu^t = \frac{e_\mu^t}{e_\mu} \quad (8)$$

and  $(:::)$  are the  $3j$  symbols. The  $e_\mu$  parameters are the mean values of the AOM parameters averaged over  $t$ . Their introduction into Eq. (6) is one of the possible solutions of the problem of several sets of intrinsic parameters in the case of non-equivalent ligands. Note, that if  $W_{kq}^\mu$  and  $s_\mu^t$  given by Eqs. (7-8) are inserted into Eq. (6), then the averaged  $e_\mu$ 's cancel out. Moreover, the ratios  $s_\mu^t$  can be treated as parameters of the model instead of  $e_\mu^t$ 's. From the algebraic point of view, this is only a scaling of the parameters without loss of generality. In practice, it is possible to estimate the ratios independently (this question is discussed later) and to consider the averaged quantities  $e_\mu$  to be adjustable parameters. The  $W_{kq}^\mu$  coefficients absorb all information about the geometry of the coordination polyhedron whereas the ratios  $s_\mu^t$  encode differences in the AOM parameters due to the individual  $ML_t$  distances. The distance dependence of  $s_\mu^t$  has the exponential character<sup>5</sup>, yet, within a limited range of distances, it is fairly well approximated by the simple power function:

$$s_\mu^t = \left( \frac{R}{R_t} \right)^{\alpha_\mu} \quad (9)$$

with the power exponents  $\alpha_\mu$  taking values in the range 4.3 to 8.9 in the case of actinide ions and simple ligands.<sup>5,10,20</sup>

An extension of the above equations to arbitrary number of different anions is straightforward. Note that the partitioning (3) neglects the contribution from the outside of the coordination cluster. This contribution and also other effects, which cannot be represented in the form of decomposition (3), are included explicitly in the enhanced model presented below.

AOM reduces the number of adjustable parameters describing the CF effect to three. The strength of the model stems from the fact that the local inter-ion interaction parameters,  $e_\mu$ , may be regarded as quantities characteristic for a given metal-ligand ( $ML_t$ ) pair. They allow one to verify unphysical solutions generated by false

minima of the fitting procedures in the standard parametric analysis on the one hand and to indicate the ensuing approximations in the case of especially complex systems, on the other. Due to the dominant character of the renormalization terms (see section II C and Eq. (14)), the AOM parameters  $e_\sigma$  and  $e_\pi$  manifest several characteristic properties:<sup>4,5,10,13,20,27</sup>

(i) their values reflect the spectrochemical ordering of the anions and

(ii) decrease slightly with increasing atomic number along the lanthanide and actinide series and, independently, with decreasing oxidation number of the metal ion,

(iii)  $e_\sigma > e_\pi > |e_\delta|$ ,

(iv)  $e_\mu^t/e_\mu^{t'} \approx \text{const.}$  for two different  $ML_t$  and  $ML_{t'}$  systems ( $t \neq t'$ ),

(v)  $e_\pi^t/e_\sigma^t \approx \text{const.}$  for a given  $ML_t$  pair,

(vi) the  $e_\delta$  parameter, usually of minor importance, has been shown to be 'lattice sensitive'<sup>5</sup> if obtained from the fitting of the experimental data. For this reason, transferability of  $e_\delta$  between various compounds seems to be questionable in the conventional AOM.

Even though exceptions from the above rules happen (see the next section), they may serve as an instructive test of any set of CF parameters determined from the experimental data. This concerns not only the fitting results obtained with other approximate models but also the basic  $B_{kq}$  parameters, which can be "translated" to  $e_\mu$  using Eq. (6) and a standard least squares procedure.

As mentioned, one of the most widely applied approximate methods, the Newman superposition model,<sup>6,13</sup> is based on the same assumptions as AOM. However, the role of intrinsic parameters is played by the  $B_{kq}$  parameters for a separated linear ligator in a local coordinate system. Due to the assumed cylindrical symmetry of each  $ML$  subsystem, only the parameters with  $q = 0$  are effective. They are denoted hereafter as " $b_k$ " to distinguish them from the  $B_{k0}$  parameters in the global coordinate system. The relation between the two sets of intrinsic parameters, AOM and SPM, can be easily obtained from Eqs. (6,7,8) by rewriting them for the specific case of the separated linear ligator:

$$b_k = \frac{2k+1}{7} \left[ \begin{pmatrix} 3 & k & 3 \\ 0 & 0 & 0 \end{pmatrix} \right]^{-1} \times \sum_{\mu=0}^3 (-1)^\mu (2-\delta_{\mu 0}) \begin{pmatrix} 3 & k & 3 \\ -\mu & 0 & \mu \end{pmatrix} e_\mu \quad (10)$$

The algebraic equivalence of the two sets of intrinsic parameters evidenced by above relation allows one to extend the literature data of their values, independently of the way in which they have been obtained.

### C. Contributions to the CF potential

The procedure outlined in subsection II A leads to several characteristic contributions to the CF potential  $V$ ,

corresponding to different mechanisms. Their discussion in next sections precedes a formulation of the enhanced angular overlap model. Thus, it is advisable to separate out these which obey the assumptions of the angular overlap model (the *AOM-consistent* contributions),  $V^{AOM}$ , and the *residuum*,  $V^{res}$ :

$$V = V^{AOM} + V^{res}. \quad (11)$$

In  $V^{AOM}$  one can further distinguish the *primary* ( $V^{pr}$ ) and *renormalization* ( $V^{ren}$ ) components:

$$V^{AOM} = V^{pr} + V^{ren}. \quad (12)$$

$V^{pr}$  represents the Coulomb interaction (direct and exchange) of the ligand electrons, and the potential of the nuclei. It diverges from the *point charge model* (pcm)<sup>1</sup> due to the *charge penetration* (cp)<sup>28</sup> and inter-ionic *exchange* (ex)<sup>29</sup> effects included in  $V^{pr}$ :

$$V^{pr} = V^{pcm} + V^{cp} + V^{ex} + V^{pr.sh}. \quad (13)$$

The intra-ionic excitations on the metal ion induced by the primary contribution lead to the AOM-consistent part of the *shielding* potential  $V^{pr.sh}$ .

$V^{ren}$  comprises the main renormalization terms implied by the ligand-metal charge transfer excitations - the *covalency* contribution,  $V^{co}$ ,<sup>6</sup> and non-orthogonality of the free-ion wave-functions localized on adjacent ions: the *overlap* contribution,  $V^{ov}$ ,<sup>6</sup> and the *contact shielding*,  $V^{cs}$ ,<sup>11</sup>:

$$V^{ren} = V^{ov} + V^{cs} + V^{co} \quad (14)$$

$V^{res}$  includes all the remaining terms. One can distinguish  $V^{nn.pol}$  - the contribution of electric multipoles induced on ligands (polarization of nearest neighbors),  $V^{fn}$  - the electrostatic potential of the point charges and electric multipoles induced on all the ions outside the cluster (electrostatic potential of further neighbors) and  $V^{res.sh}$  which symbolizes the shielding correction to these electrostatic potentials:

$$V^{res} = V^{nn.pol} + V^{fn} + V^{res.sh}. \quad (15)$$

Due to the cancellation of various terms in the primary and residual contributions,  $V^{ren}$  or  $V^{ov}$  in essence, turns out to be the most important mechanism for the ionic compounds in favor of AOM.<sup>5,6,10,13,27</sup> This corollary is supported also by the results presented in next section.

Explicit formulas for all the above contributions are given in Appendix B.

## III. AB INITIO CALCULATIONS

### A. Details of the calculations

The compounds under consideration represent a variety of the crystal structures. The point symmetry of

the metal ion varies from cubic one in  $\text{UO}_2$  (CaF<sub>2</sub> structure, space group  $Fm\bar{3}m$  - 225), through  $D_{2d}$  in  $\text{UOX}$  (PbFCl-type structure,  $P4/nmm$  - 129),<sup>30</sup>  $C_{2v}$  in  $\text{UTe}_2$  (orthorhombic space group  $Immm$  - 71),<sup>31</sup> up to  $C_s$  in  $\beta\text{-US}_2$  and  $\beta\text{-USe}_2$  (PbCl<sub>2</sub>-type structure,  $Pnma$  - 62).<sup>32</sup>

Zero-order free-ion wave-functions have been generated using self-consistent Dirac-Slater procedure ATOM<sup>33,34</sup> with the stabilizing potential well determined by the Madelung energy.<sup>35</sup> The calculations have been performed in the crystallographic coordinate system. The lattice sums of static and induced multipoles generated by the set of the crystal electrostatic equilibrium equations (B13) in Appendix B have been calculated according to Eq. (B12) using a modified version of the program CHLOE.<sup>14,36</sup> and multipole polarizabilities from Ref. 37. The summation in the multipole expansion (B12) was limited to monopoles, dipoles and quadrupoles ( $n = 0, 1, 2$ ) in the present calculations. The effect of the outer electrons occupying the  $6s$  and  $6p$  closed shells of the metal ion have been estimated via Sternheimer's shielding factors,  $\sigma_k$ , scaling the corresponding  $B_{kq}$ 's<sup>38,39</sup>. The charge penetration, exchange and renormalization terms have been calculated using the program LF developed for the  $f$ -electron compounds.<sup>40</sup>

The free-ion part of the effective Hamiltonian contains the intraionic Coulomb repulsion of the  $5f$  electrons of the  $\text{U}(4+)$  ion, controlled by the Slater integrals  $F^k$ ,  $k = 2, 4, 6$ , spin-orbit coupling with the  $\zeta_{5f}$  parameter and further corrections of higher order (see Appendix A). The "free-ion" parameters depend on the crystal, in which the metal ion is embedded, and may vary in certain range, modifying the inter-term spacing.<sup>41</sup> Fortunately, these differences are limited and they have rather negligible impact on the splitting of the ground multiplet. Thus, we adopt the values obtained earlier from the fitting of the optical spectra for  $\text{U}^{4+}$  in  $\text{ThGeO}_4$  (in meV):<sup>42</sup>  $F^2 = 5339$ ,  $F^4 = 4833$ ,  $F^6 = 3018$ ,  $\alpha = 3.72$ ,  $\beta = -81.8$ ,  $\gamma = 148.8$ ,  $M^0 = 0.124$ ,  $M^2 = 0.069$ ,  $M^4 = 0.047$ ,  $P^2 = 62.0$ ,  $P^4 = 31.0$ ,  $P^6 = 6.2$ ,  $\zeta_{5f} = 224.2$ . The calculations of the eigenvalues and eigenvectors and/or fitting of the measured energies of electronic transitions have been performed with a set of  $f$ -shell empirical computer programs developed by M. F. Reid,<sup>43</sup> supplemented with a subprogram POD<sup>40</sup> for calculation of some thermodynamic quantities.

## B. Reliability of the results

This type of *ab initio* calculations was performed previously for, among the others,  $\text{UO}_2$  and  $\text{UOS}$ ,<sup>20,21,44</sup> the compounds for which comprehensive experimental data are available, including optical and/or inelastic neutron scattering (INS) spectra.<sup>44,45,46</sup> Discrepancy of the obtained theoretical  $B_{kq}$  parameters and the phenomenological values determined by a fitting to the experimental data did not exceed 20-30%. Now the calculations are extended to the  $\text{UX}_2$  sub-series. For these compounds

the published experimental data are not so rich.<sup>32,47,48</sup> We can reproduce certain thermodynamic averages, e.g. the paramagnetic Van Vleck susceptibility (see Appendix C) depicted in Fig. 1. The corresponding energy levels are shown in Fig. 2 and they are discussed later. The experimental slope, shape and the variation of the temperature independent susceptibility at the lowest temperatures along the series agree quite well with the results of the *ab initio* calculations. A discrepancy between the theoretical and experimental lines visible for  $\text{USe}_2$  and  $\text{UTe}_2$  can be attributed to the interionic exchange not included in the model calculations. Judging from the mutual shifts of the lines, the interaction has to be of ferromagnetic type for  $\text{USe}_2$  and greater in the absolute value than the antiferromagnetic type observed for  $\text{UTe}_2$ . The first excited level lying at 8.0, 1.6 and 2.5 meV for  $\text{U}^{4+}$  ion in  $\text{US}_2$ ,  $\text{USe}_2$  and  $\text{UTe}_2$ , respectively (see Fig. 2) influences the magnetic properties of these systems with a singlet ground state. Above 20 K,  $\text{UTe}_2$  and especially  $\text{USe}_2$  behave as if they had a degenerate ground state. Relatively weak U-U exchange interaction in  $\text{USe}_2$  (U-U distance of 0.423 nm<sup>32</sup>) turns out to be sufficient to induce the long-range ferromagnetic order below 14 K.<sup>47</sup> Note, that the first excited state has the lowest energy just for this compound.  $\text{USe}_2$  is the only dichalcogenide that orders magnetically.<sup>32</sup> No ordering in  $\text{UTe}_2$  with the shortest U-U distance 0.378 nm may be due to the fact that only one of seven neighboring uranium ions is placed at that distance, whereas the remaining four are placed at 0.490 nm and two at 0.416 nm. A different curvature of the theoretical and experimental reciprocal susceptibilities observed for  $\text{USe}_2$  below 60 K may be ascribed to the magnetic fluctuations increasing with temperature approaching the critical point, which were not taken into account in the model calculations. The effective magnetic moments, of 2.94 BM, 3.01 BM and 3.09 BM, are lower than those derived from the experimental curves, of 3.25 BM 3.20 BM and 3.21 BM, reported for  $\text{US}_2$ ,  $\text{USe}_2$ <sup>47</sup> and  $\text{UTe}_2$ ,<sup>48</sup> respectively.

Figure 2 shows the splitting of the ground term  $^3H_4$  of the  $\text{U}^{4+}(5f^2)$  ion in the  $\text{UX}_2$  series, obtained by simultaneous diagonalization of Hamiltonian (A1-A2), with the CF parameters determined from first principles shown in Table I and the free-ion parameters listed in Appendix A. These results have been employed in calculations of the temperature dependencies of the magnetic susceptibilities discussed above.  $B_{kq}$  parameters in Table I reveal no regularity along the series that might be expected, for instance, from the spectrochemical ordering of ligands. This observation is not only a consequence of the inherent ambiguity of the CF parametrization in low symmetry systems.<sup>49</sup> It would be difficult to find any trend also for the energy levels shown in Fig.2. Analogous behavior of the  $\text{AnOX}$  series has been ascribed to an influence of the competing oxygen and chalcogenide groups in the  $W_{kq}^\mu$  coefficients (7).<sup>20,21</sup> Now it becomes evident that also in the case of one type of anions the coordination geometry may obscure the expected regularities so

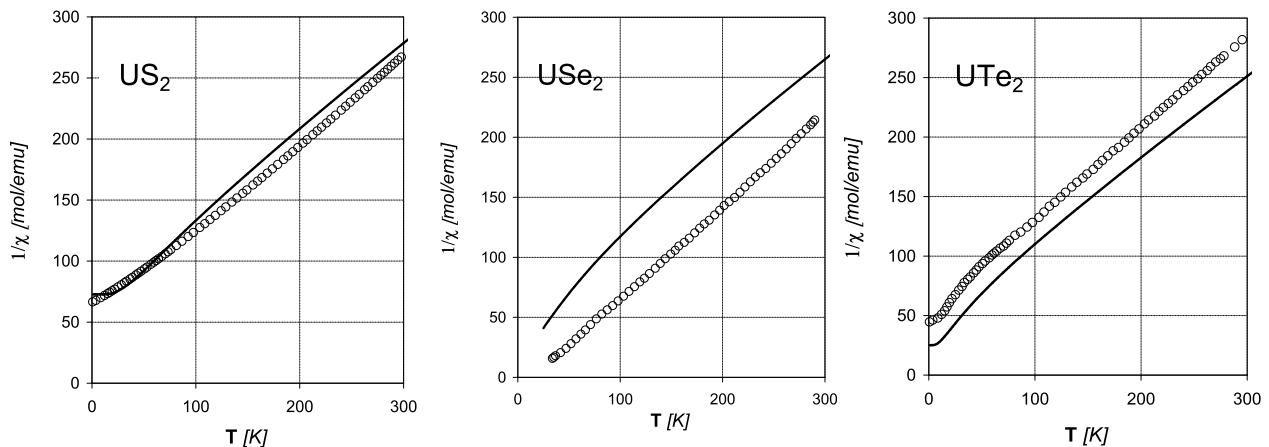


FIG. 1: Reciprocal magnetic susceptibilities of powdered dichalcogenides as a function of the temperature: comparison of the experimental (open circles)<sup>32,47,48</sup> and theoretical (continuous lines) curves obtained using the Van Vleck formula (C1).

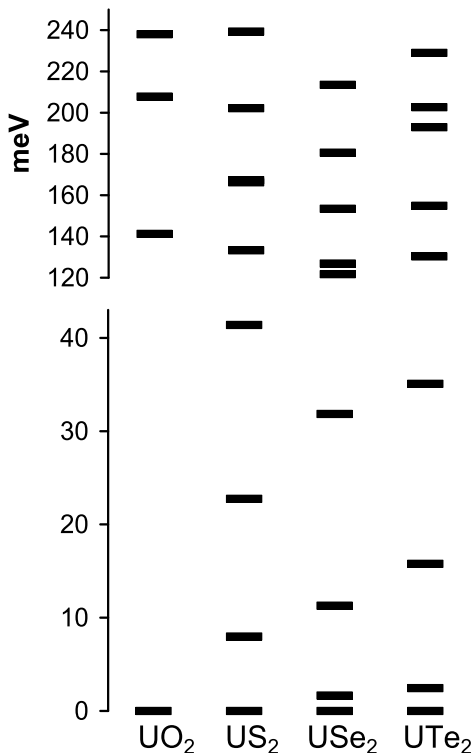


FIG. 2: Splitting of the uranium (4+) ground term  ${}^3H_4$  in the  $UX_2$  crystals obtained by simultaneous diagonalization of Hamiltonian (A1-A2) with the CF parameters determined from first principles. The lower part of the diagram uses the scale enlarged several times as compared with that for the upper part.

clearly manifested, on the other hand, by the intrinsic AOM parameters (cf. Table II). As we see in next section, possible trends in CFP sets revealed elsewhere using an independent method based on certain conserved quantities associated with CF parameters<sup>50</sup> may be governed by the AOM-consistent part of crystal field.

### C. AOM-consistent part of crystal field

The results displayed in Table I are indicative of an essential meaning of the AOM-consistent contributions. Nevertheless they also show that the residual contribution may become crucial for some parameters as in the case of  $B_{44}$  for  $US_2$  or  $B_{22}$  for  $UTe_2$ . More detailed data, which are presented in Table I for  $USe_2$ , give some idea about the role of the particular CF mechanisms. Mutual compensation of the various primary components and importance of the renormalization terms is clearly manifested there. Handling each non-equivalent  $ML$  pair independently in compounds like  $US_2$  (with six different  $ML_t$  distances and two non-equivalent crystallographic positions of the sulphur ion) would multiply the number of the intrinsic parameters, making the model practically intractable. Usually, the dependence of the intrinsic parameters  $e_\mu$  (or their renormalized counterparts  $s_\mu$  (8)) on the  $ML$  distance,  $R$ , is assumed to have a definite character<sup>13,20</sup>. In a limited range of distances around an average value for a given  $ML$  bond, it is approximated by the power function (9). The power exponents,  $\alpha_\mu$ , are treated then as an additional characteristic of the  $ML$  bond that allows one to maintain the minimal number of independent parameters.

The simulations of the  $e_\mu(R)$  functions have been performed for all the uranium linear ligators occurring in the series  $U^{4+} - X^{2-}$ . As Eqs. (B4-B10) in Appendix B show, the functions are determined by squares of metal-ligand overlap integrals and Madelung energies of the ions

TABLE I: *AOM-consistent* (12) and *residual* (15) contributions to the CF parameters calculated from first principles for the  $UX_2$  series in the crystallographic coordinate systems.<sup>51</sup> The primary contribution  $V^{pr}$  (13), renormalization term  $V^{ren}$  (14), ligand polarization  $V^{nn.pol}$  (B12) and potential of the further neighbors  $V^{fn}$  are specified for  $USe_2$  in parentheses. All values in meV.

	$US_2$			$USe_2$			$UTe_2$				
	$V^{AOM}$	$V^{res}$	$V$	$V^{AOM}$	$(= V^{ren} + V^{pr})$	$V^{res}$	$(= V^{nn.pol} + V^{fn})$	$V$	$V^{AOM}$	$V^{res}$	$V$
$B_{20}$	65	-17	48	84	(73 + 11)	-10	(-24 + 14)	74	38	13	51
$B_{21}$	-203	-3	-206	-200	(-194 - 5)	-6	(-1 - 5)	-206			
$B_{22}$	-79	-6	-85	-24	(-26 + 3)	-3	(-9 + 6)	-26	28	42	70
$B_{40}$	-88	2	-86	-71	(-52 - 19)	4	(4 - 0)	-67	-436	-184	-619
$B_{41}$	82	6	88	39	(32 + 7)	-5	(0 - 5)	34			
$B_{42}$	-274	-8	-282	-264	(-297 + 33)	-16	(6 - 22)	-280	364	79	442
$B_{43}$	257	45	301	186	(236 - 49)	26	(25 + 1)	212			
$B_{44}$	-60	-51	-111	-64	(-62 - 2)	-48	(-21 - 27)	-112	74	-26	48
$B_{60}$	174	-2	172	78	(80 - 3)	1	(2 - 1)	78	87	4	91
$B_{61}$	-233	-1	-233	-230	(-311 + 82)	-1	(-1 + 0)	-231			
$B_{62}$	394	5	398	340	(441 - 101)	3	(-5 + 9)	344	11	-6	6
$B_{63}$	171	-1	170	203	(248 - 45)	-1	(-1 - 0)	202			
$B_{64}$	37	18	55	34	(59 - 26)	9	(8 + 1)	43	-122	26	-96
$B_{65}$	-369	-10	-379	-320	(-383 + 63)	-4	(-4 - 0)	-324			
$B_{66}$	243	9	252	212	(262 - 50)	6	(2 + 4)	219	-151	0	-151

TABLE II: Results of ab initio calculations of the AOM parameters (in meV) corresponding to the *AOM-consistent* part of the CF potential for various  $An^{4+} - X^{2-}$  systems and the average inter-ion distances  $R_{av}$ .

	$R_{av}$ [nm]	$e_\sigma$	$e_\pi$	$e_\delta$
U <sup>4+</sup> -O <sup>2-</sup> in:				
UO <sub>2</sub>	0.237	350	209	64
UOS <sup>b</sup>	0.234	340	211	63
UOSe <sup>b</sup>	0.236	324	196	55
UOTe <sup>b</sup>	0.237	316	186	46
U <sup>4+</sup> -S <sup>2-</sup> in:				
UOS	0.293	211	96	32
US <sub>2</sub>	0.289	265	102	36
U <sup>4+</sup> -Se <sup>2-</sup> in:				
UOSe	0.304	204	91	31
USe <sub>2</sub>	0.301	240	88	30
U <sup>4+</sup> -Te <sup>2-</sup> in:				
UOTe	0.325	185	90	31
UTe <sub>2</sub>	0.317	190	88	29
Np <sup>4+</sup> -O <sup>2-</sup> in:				
NpO <sub>2</sub>	0.235	317	186	56
NpOS	0.233	304	181	53
NpOSe	0.235	291	169	47
Np <sup>4+</sup> -S <sup>2-</sup> in:				
NpOS	0.291	191	87	30
Np <sup>4+</sup> -Se <sup>2-</sup> in:				
NpOSe	0.302	183	82	29

<sup>b</sup>From Ref. 20.

in crystals. To ensure comparability of the results obtained for different  $ML$  pairs, a virtual  $ML_2$  crystal of the  $CaF_2$  structure has been employed, where ligands form a cube with its center occupied by the metal ion. The Madelung potential at the  $L$  and  $M$  sites in this structure is given by the formulae:  $U^L = -8.14e/a$  and

$U^M = 15.13e/a$ , respectively, whereas the lattice constant  $a$  is related to the  $ML$  distance  $R$  by the expression  $R = \sqrt{3}a/4$ . The intrinsic parameters depend on  $U^L$  and  $U^M$  in a non-trivial way through the zero-order wave-functions and explicitly due to the renormalization terms (B4, B6). This implies the use of different free-ion wave-functions for each  $R$ . The calculations have been performed for seven values of  $R$  distributed uniformly between 0.18 nm and 0.40 nm. The radius  $D$  of the stabilizing potential well for the negative ions of the  $U^L$  depth has been assumed to be equal to  $-2e/U^L$ .

The results are shown in Fig. 3. Due to the predominating renormalization terms (cf. Fig. 4), the  $e_\mu(R)$  functions have an exponential character for the  $ML$  distances around the average values. For larger distances, where the electrostatic contributions dominate, they take a form of a polynomial. The slope of  $e_\sigma(R)$  decreases in the limit of short distances, more visibly on going from the oxide to telluride. The function  $e_\sigma(R)$  reaches even a maximum for the  $U^{4+}$ - $Te^{2-}$  bond. Fig. 4 indicates that the importance of the charge penetration rapidly increases as compared with that for other mechanisms. Since this contribution has opposite sign for  $e_\sigma$  and  $e_\pi$ , the ratio  $e_\pi/e_\sigma$  increases in the limit of small distances.

A similar behavior, although not so evident, can be deduced from the data presented in Table II of Ref. 52 for the  $Pr^{3+}$ - $Cl^-$ , if the Coulomb contributions are scaled using the Sternheimer shielding factors and the SPM parameters are converted into the AOM ones by Eq. (10). An open question is whether the observed increase of the  $e_\pi/e_\sigma$  ratio at the lowest distances characteristic for dense systems is a true property of metals. We may only note that analogous distance dependencies of the AOM parameters for the  $Sm^{2+}$ - $Cl^-$  and  $Sm^{2+}$ - $F^-$  systems derived from the data reported in Ref. 53 did not confirm

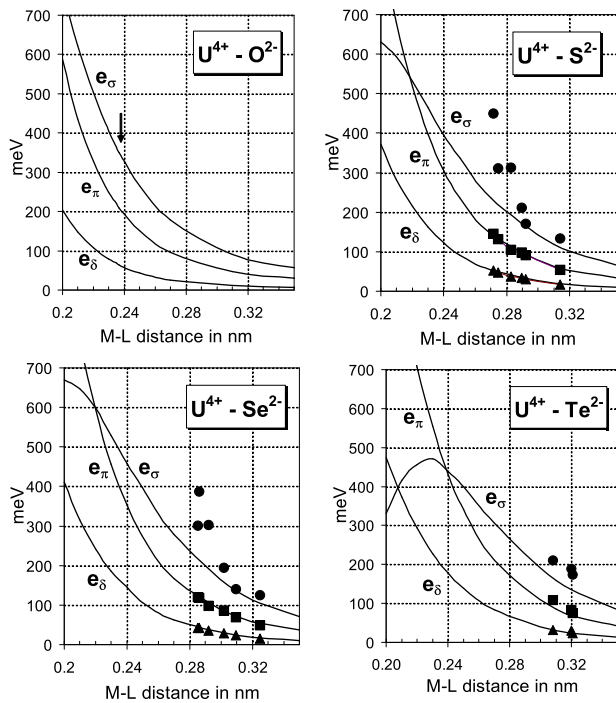


FIG. 3: Dependence of the inter-ion effective interaction parameters of the angular overlap model on metal-ligand distance for the  $U^{4+} - X^{2-}$  pairs in a hypothetical crystal of  $CaF_2$  structure. The circles, squares and triangles represent actual intrinsic parameters  $e_\sigma$ ,  $e_\pi$  and  $e_\delta$  obtained for  $UX_2$ .

this conjecture.

The model calculations taking into account the variation of Madelung energy with the  $ML$  distance lead to lower values of the power exponents  $\alpha_\mu$  as compared with earlier estimations.<sup>20</sup> The AOM parameters determined for the actual crystals  $AnOX$  and  $AnX_2$  are listed in Table II and shown in Fig. 3. Each  $ML$  distance occurring in these compounds is represented in Fig. 3 by three points corresponding to the  $e_\sigma$ ,  $e_\pi$ , and  $e_\delta$  parameters. We see that they do not follow the smooth lines discussed above. The crucial  $e_\sigma$  parameter turns out to be simultaneously the most irregular one. This is because it reflects the discontinuity of the Madelung potential most. In light of the present calculations, the properties (i-v) of the AOM parameters specified in section II B should be treated with caution not only because of very existence of the residual contributions but also because of the revealed here inherent irregularity of the AOM-consistent contributions.

## IV. ENHANCED ANGULAR OVERLAP MODEL

### A. Formulation

In view of apparent irregularity of the AOM parameters and the erratic behavior of the residual contribution

(15) discussed in the preceding section and manifested in Fig. 3 and Table I we propose to link the phenomenological AOM approach with the *ab initio* calculations in the enhanced angular overlap model (EAOM). Our model assumes each ordinary CF parameter to be composed of two components: the main, adjustable one, parametrized according to Eqs. (6-8) and the fixed residuum,  $B_{kq}^{res}$  corresponding to the potential (15), determined from Eq. (B12):

$$B_{kq} = \sum_{\mu} W_{kq}^{\mu} e_{\mu} + B_{kq}^{res} \quad (16)$$

with  $e_{\mu}$  playing the role of the phenomenological EAOM parameters. The separation of the residual, off-AOM contribution from the global CF parameters supports a more precise and consistent AOM parametrization of the remainder. In consequence, the intrinsic character of the corresponding EAOM parameters is genuinely maintained. EAOM is not much more complicated than the parental AOM but the main inherent shortcoming of the latter is removed by excluding explicitly the off-AOM contributions from the simplified phenomenological treatment. These off-AOM contributions are estimated in our model from the first principles. Note, that very construction makes the model exact (at least in the frames of the one-electron approximation) provided the off-AOM contributions are determined precisely, what, of course, is hardly possible.

The AOM-consistent contributions listed in Table II can be regarded as a crude theoretical estimation of the EAOM parameters. Their more accurate determination requires an involved self-consistent approach to account for the energy-dependent parameter-renormalization terms.<sup>4</sup> Thus, treating this part of the CF potential as a phenomenological quantity allows one to handle these self-energy effects in the simplest possible way.

Naturally, the EAOM parameters obtained from the fitting of the observed electronic energy levels cannot have the same values as the AOM parameters derived from the analogous fitting within the conventional AOM approach. Moreover, the rules (i-v) observed for the usual AOM parameters (see section II B) seem more justifiable in the case of the theoretical, AOM-consistent contributions and thus, also for the EAOM parameters. Nevertheless, in light of the calculations presented in section III C, still they remain acceptable in a rather limited range of the  $ML$  distances, in vicinity of their averaged values.

Compounds containing several groups of symmetry-equivalent ligands require the  $s_{\mu}^t$  ratios in the geometrical coefficients  $W_{kq}^{\mu}$  (7) to be determined. The observed above (see section III C and Fig. 7) irregularity of the EAOM parameters due to, among the others, the Madelung energy, can be reproduced in the model by employing the *ab initio* values of these ratios. Thus, it is advisable to calculate  $s_{\mu}^t$ 's for each individual  $ML_t$  pair rather than applying the approximation (9).



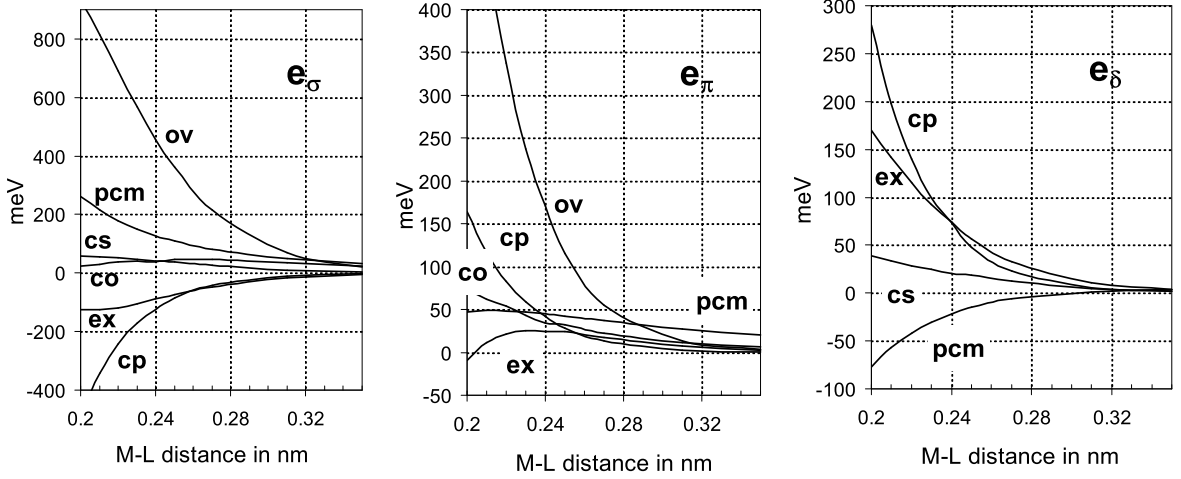


FIG. 4: Distance dependence of the main contributions to the  $e_\mu$  parameters: point charges ( $pcm$ ), overlap ( $ov$ ), covalency ( $co$ ), charge penetration ( $cp$ ), exchange ( $ex$ ), contact shielding ( $cs$ ).

The same theoretical calculations may also be employed to formulate further, more restrictive parametrizations, which may be helpful in the case of the most complicated experimental data. For instance, fixing both the ratios

$$s_{\mu\sigma} = e_\mu/e_\sigma, \quad \mu = \pi, \delta \quad (17)$$

equal to their theoretical values leads to a single-parameter version of the model:

$$B_{kq} = B_{kq}^{res} + \widetilde{W}_{kq} \tilde{e} \quad (18)$$

with

$$\begin{aligned} \widetilde{W}_{kq} = & \frac{2k+1}{7} \left[ \begin{pmatrix} 3 & k & 3 \\ 0 & 0 & 0 \end{pmatrix} \right]^{-1} \sum_{\mu} (-1)^{\mu} (2 - \delta_{\mu 0}) \times \\ & \times \begin{pmatrix} 3 & k & 3 \\ -\mu & 0 & \mu \end{pmatrix} \sum_t C_q^{(k)*}(\Theta_t, \Phi_t) s_\mu^t s_{\mu\sigma} \quad (19) \end{aligned}$$

The  $\tilde{e}$  parameter in Eq. (18) corresponds directly to  $e_\sigma$  but also the  $e_\pi$  and  $e_\delta$  contributions enter into the model through the  $s_{\mu\sigma}$  ratios in the above  $\widetilde{W}_{kq}$  coefficients. Hence, a variation of  $\tilde{e}$  modifies also the  $e_\pi$  and  $e_\delta$  contributions to the crystal field in proportions given by  $s_{\mu\sigma}$ . Note, that Eq. (18) without the residual part would be a simple scaling of the crystal field effect predicted by the AOM-consistent part of the *ab initio* calculations.

An intermediate, two-parameter version of the model can be defined in several ways by fixing any of the  $s_{\mu\sigma}$  ratios or their combinations. These single- and two-parameter versions, should not be confused with models commonly employed for the transition elements<sup>4,13</sup> which omit simply the  $\pi$  and  $\delta$  contributions or only the  $\delta$  contribution.

Generalization of the model and the equations (16-19) to systems containing different ligands is straightforward (see the example given below).

## B. Applications

Due to the highly reduced number of the free parameters (up to the single-parameter version, Eq. (18)), the simplified EAOM parametrizations of the CF effect may be especially helpful in all these cases of incomplete or more complicated experimental data so frequently met in the most interesting  $f$ -electron systems. Three possible types of applications of EAOM are exemplified in what follows.

The first one, already discussed in Ref. 21, concerns interpretation of certain magnetic properties of NpOX where  $X = O, S$  and  $Se$ . The procedure might be seen as a general method of interpretation of the electronic properties based on transferability of the intrinsic parameters between different compounds, using the phenomenological CF parameters for the specimens assumed to be known, i.e. the compounds, the electronic structure of which is believed to be reliably determined. In the example under consideration, the parameters  $(B_{kq})^U$  reported for  $UO_2, UOX$ , the ones of the most widely investigated uranium compounds, were employed.<sup>20,44</sup> The corresponding AOM parameters  $e_\mu^{UO}$  and  $e_\mu^{UX}$  were determined from system of equations (16) and its version adapted to two different ligands, oxygen and chalcogenide,

$$B_{kq} = B_{kq}^{res} + \sum_{\mu} \left( W_{kq}^{\mu,O} e_\mu^O + W_{kq}^{\mu,X} e_\mu^X \right) \quad (20)$$

exploiting the *ab initio* values of the  $s_\mu^t$  ratios. In the second phase, the procedure was reversed to estimate unknown CFP's for the less explored experimentally neptunium oxychalcogenides. First, the  $e_\mu^{NpO}$  and  $e_\mu^{NpX}$  parameters were derived by scaling their uranium counterparts in terms of the ratios of the corresponding theoretical values:  $(e_\mu^{NpX}/e_\mu^{UX})_{calc}$ . The  $B_{kq}^{Np}$  parameters

obtained, again, from Eqs. (16, 20) were, in the final step, adjusted to match the experimental values of the ordered magnetic moments. In this phase, a simultaneous diagonalization included, apart from the CF Hamiltonian and the "free-ion" interactions, the intermetallic exchange interaction in the zero-temperature mean-field approximation. The magnetic properties of the neptunium oxychalcogenides, including the anisotropic ground state magnetic moment, the temperature dependencies of the paramagnetic susceptibility and the magnetization at 0 K, were described satisfactorily in this approach (see Ref. 21 for further details). The example illustrates efficiency of the method based on EAOM in interpretation of the electronic structure in the case of inconclusive experimental data. The intrinsic parameters collected in Table II, may serve as a tentative source of the relations between them in further applications of EAOM.

The second example concerns interpretation of the thermodynamic and magnetic properties<sup>54,55</sup> and inelastic neutron scattering (INS) spectra of UOS.<sup>46,56</sup> In the analysis of the experimental data,<sup>20</sup> the initial energy levels assignment was deduced on the grounds of first-principles calculations. The fitting of the INS data<sup>46,56</sup> was performed in two steps. First, the AOM was applied to obtain the identified INS transition energies. Subsequent refinement of the corresponding usual CF parameters yielded agreement with the remaining experimental data.<sup>46,54,55</sup> A special attention was paid to the ordered magnetic moment  $\mu_{ord}$  and relative intensities of the INS transitions. However, the problem with the infinite number of acceptable solutions could not be resolved. Namely, the experimental data for this tetragonal  $C_{4v}$  system could be satisfactorily reproduced with any value of the  $B_{20}$  in the range of  $-50$  to  $-223$  meV, provided the remaining parameters,  $B_{40}$ ,  $B_{44}$ ,  $B_{60}$ ,  $B_{64}$  were simultaneously adjusted to the given  $B_{20}$ . Some features of the electronic structure were varying with the CF parameters in this ambiguity range but they were not detectable in  $\mu_{ord}$  and in the position and shape of the most intense INS lines below 100 meV. In addition, it was demonstrated<sup>20</sup> that the INS excitations to two of the highest levels of the  ${}^3H_4$  term,  $\Gamma^2$  and  $\Gamma^{1(2)}$ , could be invisible if  $B_{20}$  had decreased below  $-146$  meV under actual incident neutron energy and angle, just as it was observed. Eventually, the set of  $B_{kq}$  parameters corresponding to the threshold value of  $B_{20} = -146$  meV was accepted as the closest one to the initial estimation.

The above problem disappears if EAOM is applied with its inherent constrains. To start with, the single-parameter version of EAOM, Eq. (16), is adapted to account for the two different anions occurring in the coordination sphere - the oxygen and sulphur:

$$B_{kq} = B_{kq}^{res} + \widetilde{W}_{kq}^O \tilde{e}^O + \widetilde{W}_{kq}^S \tilde{e}^S \quad (21)$$

with coefficients  $W$  given by Eq. (19),  $B_{kq}^{res}$  and the remaining data taken from Ref. 20. It turns out that this simplest version of EAOM, with only two effective parameters  $\tilde{e}^O$  and  $\tilde{e}^S$ , describes fairly well the three elec-

tronic INS transitions:<sup>46,56</sup> 74 meV ( $\Gamma^5(1) \rightarrow \Gamma^3$ ), 83 meV ( $\Gamma^5(1) \rightarrow \Gamma^4$ ), and 87 meV ( $\Gamma^5(1) \rightarrow \Gamma^5(2)$ ). These intervals can be easily matched by a minor refining of the *ab initio* ratios  $s_{\pi\sigma}$ . Figure 5 (c) shows the resulting energies and the transition probabilities estimated in terms of the squares of the matrix elements of the Zeeman operator between the initial and final states.<sup>57</sup> The Debye-Waller and 5*f*-electron form factors are not taken into account since we are interested only in comparison of various numerical simulations without a direct reference to the experimental recordings. The Gaussian shape of the figured transitions have only an illustrative character. The present simulation of the INS transitions does not differ much from the previous one shown in Fig. 5 (b).<sup>20</sup> Taking into account a finite width of the experimental lines and limited range of the measurable energies both the simulations seem acceptable. In particular, the main lines around 80 meV are quite similar to the measured ones.<sup>46,56</sup> The line at about 40 meV was neither observed nor excluded by the experimental data since it is relatively weak and lies in the region of the phonon sidebands. The ordered magnetic moment of 2.11 MB as determined from the obtained wave-functions, is higher than the observed one of 2.00 MB.<sup>55</sup> Nevertheless it can be reduced to about 2.04 BM due to the overlap and covalency effects.<sup>58</sup> Our phenomenological results can be compared with *ab initio* predictions. The parameter  $\tilde{e}^O = 370.2$  meV is about 10% higher than the theoretical value of  $e_\sigma$  from Table II, whereas  $\tilde{e}^S = 157.1$  meV is lower than its counterpart. The differences between the corresponding phenomenological and theoretical parameters become even more pronounced in the case of the  $B_{kq}$  parameters listed in Table III. Taking into account inherent limitations of the *ab initio* calculations due to numerous approximations and uncertainty of the Sternheimer shielding factors, dipole and quadrupole polarizabilities, such a divergence seems inevitable. We assume the ratios of the theoretical values of the EAOM parameters, (8, 17), used in formulation of the approximate phenomenological models, Eqs. (16, 18), to be more reliable than the theoretical parameters themselves because of an expected partial cancellation of the calculation errors. The present EAOM values of the  $B_{kq}$  parameters lie between those obtained using the conventional AOM and the refined model from Ref. 20. The divergence between the sets of the phenomenological parameters, especially between these in the two last lines of Table III, is moderate. Further INS investigations with higher incident neutron energies could decisively verify the predicted positions of the  $\Gamma^2$  and  $\Gamma^{1(2)}$  levels.

The low symmetry crystals,  $UX_2$ , considered in section IIIB may serve as a next example of application of EAOM. The model allows one to reduce 15 ( $US_2$ ,  $USe_2$ ) or 9 ( $UTe_2$ )  $B_{kq}$  parameters specific for the point group symmetries in these compounds to only 1-3 EAOM parameters. Note, that very construction of any version of EAOM, including the single-parameter one, Eq. (18), ensures accuracy of the electronic structure simulation not

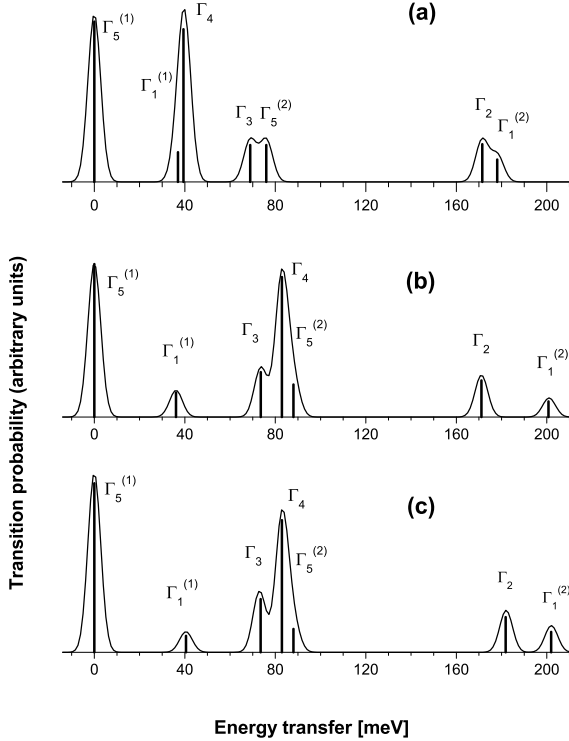


FIG. 5: Simulation of the INS spectra of UOS in various crystal field models: (a) - *ab initio* calculations, (b) - refined model from Ref. 20, (c) - EAOM.

TABLE III: Comparison of various  $B_{kq}$  sets obtained for UOS (in meV).

	$B_{20}$	$B_{40}$	$B_{44}$	$B_{60}$	$B_{64}$
<i>Ab initio</i> calculations	-180	-545	-119	424	104
AOM	-117	-567	-11	632	250
Model from Ref.20	-147	-579	-39	595	447
EAOM	-159	-624	-21	627	380

worse than that obtained from the *ab initio* calculations. This is because the *ab initio* calculations determine not only the starting values of the parameters but also the coefficients  $W$  and residual off-AOM terms in Eqs. (16,18). Thus, with EAOM one can try to reproduce the electronic structure of any compound even if the available experimental data are limited merely to a single thermodynamic characteristic like the magnetic susceptibility discussed in section III B. In the specific case of  $UX_2$ , the theoretical curves displayed in Fig. 1 represent simultaneously the initial phenomenological dependencies in our model. The corresponding EAOM parameters listed in Table II are thus the natural and right starting values in subsequent steps of the further interpretation of the electronic structure.

## V. CONCLUDING REMARKS

The crystal field potential in the quasi-phenomenological enhanced angular overlap model (EAOM) proposed here is divided into two parts: the main part, adjustable, which comprises the contributions amenable to the conventional AOM parametrization and the residual one, fixed, representing all the remaining terms. The fixed, off-AOM residual part contains the electrostatic contributions of further neighbors and the ligand polarization contribution, accuracy of determination of which hinge on the available ionic polarizabilities and the shielding factors. Much more complicated renormalization terms in the CF potential are handled in the phenomenological way together with the core, charge penetration and interionic exchange contributions. The parametrization applied is known from the usual AOM approach. Its simplicity is a consequence of the axial local symmetry of the encoded contributions and their additivity.

Aptness of such a discrimination between the contributions is illustrated by an increasing amount of examples of first principles calculations in the literature and also by the results presented in this paper. Additionally, the calculations provide the ratios of the intrinsic parameters which may be employed in further applications of EAOM. The simulations performed for the virtual  $UX_2$  crystal of  $CaF_2$  symmetry give an idea about dependence of the EAOM parameters on metal-ligand distance. They show the evolution of the mutual relations between the AOM-consistent contributions. The observed behavior of the AOM-consistent contributions to the intrinsic parameters in the limit of the shortest metal-ligand distances touches a more complex problem of the CF effect in metallic systems. A comparison of these simulation with the *ab initio* calculations for the actual  $UX_2$  compounds evidences certain volatility of the intrinsic parameters. It turns out that the assumption, commonly accepted for models based on the superposition ansatz (conventional AOM or SPM and their various modifications), saying that the intrinsic parameters are smooth functions of metal-ligand distance is not always valid due to various Madelung energies of the ions in the real crystals and a high sensitivity of the intrinsic parameters to these energies. This points to necessity of enforcing each particular implementation of the phenomenological model with the *ab initio* calculations for an actual specimen just as it is postulated in EAOM.

EAOM ensures a highly compact description of the electronic structure of even so complex ionic systems as the actinide crystals. The examples discussed in the paper represent various kinds of conceivable applications. The case of experimental data limited to only certain magnetic characteristics of systems of low crystal symmetries is illustrated for the  $UX_2$  series. In other example, the electronic structure for the  $NpOX$  is predicted by transforming the intrinsic parameters for the corresponding  $UOX$  compounds and exploiting relations between

the parameters calculated *ab initio*. Various experimental data are available in the case of UOS. They include the magnetic and thermodynamic properties as well as the inelastic neutron scattering spectra. Nevertheless, the electronic structure cannot be resolved within the conventional CF parametrization scheme without additional assumptions of rather heuristic nature. EAOM is shown to be capable of describing of all of the observed properties unequivocally.

EAOM is open for further improvements. We mention here about a more accurate potential that could be obtained from the lattice self-consistent calculations<sup>4,10</sup> to correct the zero-order wave-functions used in the calculations. Direct evaluation of multipole polarizabilities and shielding factors for a given specimen may be important for calculations of the residual part of the crystal field, since these quantities depend on the Madelung energies of the ions.<sup>37</sup> Perhaps, an analogous idea of partitioning of the CF potential into phenomenological and fixed parts may be also applied to much more complicated metallic systems.

### Acknowledgments

The author thanks prof. Robert Troć (ILT&SR, Wrocław) for providing the source recordings of the susceptibility data for UX<sub>2</sub>, dr. Michael F. Reid (University of Canterbury, Christchurch, New Zealand) for the f-shell programs, dr. Michelle Faucher (Clamart, France) for the CHLOE program and prof. Jacek Mulak (ILT&SR, Wrocław) for careful and critical reading of the manuscript, .

### APPENDIX A:

The parametric Hamiltonian<sup>10,23,59</sup> contains the free-ion, spherically symmetric part,  $H_0$ , and crystal-field potential,  $V$ ,

$$H = H_0 + \sum_i V(\mathbf{r}_i/r_i), \quad (\text{A1})$$

where the summation index  $i$  runs over all  $f$ -electrons. The free-ion part can be written as follows:

$$\begin{aligned} H_0 = & E_{ave} + \sum_{k=2,4,6} F^k(nf, nf) f_k + \zeta_{5f} A_{SO} + \\ & \alpha L(L+1) + \beta G(G_2) + \gamma G(R_7) + \\ & \sum_{k=0,2,4} M^j m_j + \sum_{k=2,4,6} P^k p_k \end{aligned} \quad (\text{A2})$$

where  $E_{ave}$  is the spherically symmetric one-electron part of the Hamiltonian,  $F^k(nf, nf)$  and  $\zeta_{5f}$  represent the radial integrals due to the electrostatic and spin-orbit interactions, while  $f_k$  and  $A_{SO}$  are the angular operators corresponding to these interactions, respectively. The  $\alpha$ ,

$\beta$  and  $\gamma$  parameters are associated with the two-body correction terms.  $G(G_2)$  and  $G(R_7)$  are Casimir operators for the  $G_2$  and  $R_7$  groups and  $L$  is the total orbital angular momentum. The electrostatically correlated spin-orbit perturbation is represented by the  $P_k$  parameters and those of the spin-spin and spin-other-orbit relativistic corrections by the  $M_j$  parameters. The operators associated with these parameters are designated by  $m_j$  and  $p_k$  respectively.

### APPENDIX B:

Main contributions to the one-electron CF potential in non-metallic crystals are listed here. For derivations and a detailed discussion see Ref. 10. Some numerical questions related to multicenter integrals and summation of weakly convergent infinite series are dealt with in Refs. 11,14,29.

From definition, the AOM-consistent part of the CF potential and thus the AOM-consistent contributions in Eqs. (13-14) are partitioned due to ligands according to Eq. (3). Therefore, without lose of generality we can consider only single ligand potential  $v_t$  in the local coordinates centered at the metal site, the  $z$  axis of which is directed towards the ligand. Due to the axial symmetry of the ligand potential the orientation of the  $x$  and  $y$  axes is immaterial. Atomic units are applied throughout this section.

$$v_t^{pcm}(\mathbf{r}) = \frac{2}{|\mathbf{r} - \mathbf{R}_t|} \quad (\text{B1})$$

$$v_t^{cp}(\mathbf{r}) = \sum_{\tau} \left[ \hat{J}(\chi_{t\tau}(\mathbf{r}), \chi_{t\tau}(\mathbf{r})) - \frac{8}{|\mathbf{r} - \mathbf{R}_t|} \right] \quad (\text{B2})$$

$$v_t^{ex}(\mathbf{r}) = - \sum_{\tau} \hat{K}(\chi_{t\tau}(\mathbf{r}), \chi_{t\tau}(\mathbf{r})) \quad (\text{B3})$$

$$\begin{aligned} v_t^{ov} = & \sum_{\tau} |\chi_{t\tau}\rangle \langle \chi_{t\tau}| \left[ \langle \varphi | \hat{h}_0 | \varphi \rangle - 2\hat{h}_0 + \right. \\ & \left. + \sum_{\substack{t', \tau' \\ t' \neq t}} (\hat{h}_0 - \hat{J}(\varphi, \varphi)) |\chi_{t'\tau'}\rangle \langle \chi_{t'\tau'}| \right] \end{aligned} \quad (\text{B4})$$

$$\begin{aligned} v_t^{cs} = & \sum_{\nu} \sum_{\tau} \{ |\langle \xi_{\nu} | \chi_{t\tau} \rangle|^2 [2\hat{J}(\xi_{\nu}, \xi_{\nu}) - \hat{K}(\xi_{\nu}, \xi_{\nu})] - \\ & - 2\langle \xi_{\nu} | \chi_{t\tau} \rangle [2\hat{J}(\chi_{t\tau}, \xi_{\nu}) - \hat{K}(\chi_{t\tau}, \xi_{\nu})] + \\ & + \sum_{\substack{t', \tau' \\ t' \neq t}} \langle \xi_{\nu} | \chi_{t\tau} \rangle \langle \chi_{t'\tau'} | \xi_{\nu} \rangle \times \\ & \times [2\hat{J}(\chi_{t\tau}, \chi_{t'\tau'}) - \hat{K}(\chi_{t\tau}, \chi_{t'\tau'})] \} \end{aligned} \quad (\text{B5})$$

$$v_t^{cov} = \sum_{\tau} \frac{\tilde{h}_{t\tau} |\chi_{t\tau}\rangle \langle \chi_{t\tau} | \tilde{h}_{t\tau}}{\Delta_{t\tau}} \quad (\text{B6})$$

$\varphi_m$  and  $\xi_\nu$  in above equations denote the 5*f* and 6*s*, 6*p* orbitals of the metal ion obtained from the Dirac-Slater calculations for the free ion,  $\chi_{t\tau}$  stand for the analogous *ns* and *np* orbitals of the anion and  $m, \nu, \tau$  are the corresponding sets of quantum numbers.  $\hat{J}$  and  $\hat{K}$  are the usual Coulomb direct and exchange operators (see for instance Ref. 10),

$$\hat{h}_0 = \frac{-\nabla^2}{2} + v_0^M + \sum_t v_{0t}^L + V^{fn}, \quad (\text{B7})$$

where  $v_0^M$  and  $v_{0t}^L$  are the Dirac-Slater free-ion metal and ligand potentials.

$$\tilde{h}_{t\tau} = h_{t\tau} - \sum_{t'\tau'} \sum_{t''\tau''} |\chi_{t'\tau'}\rangle \langle \chi_{t'\tau'} | h_{t\tau} | \chi_{t''\tau''}\rangle \langle \chi_{t''\tau''} | \quad (\text{B8})$$

$$h_{t\tau} = h_0 - \hat{J}(\chi_{t\tau}, \chi_{t\tau}) \quad (\text{B9})$$

$$\Delta_{t\tau} = \langle \varphi | h_{t\tau} | \varphi \rangle - \langle \chi_{t\tau} | h_0 | \chi_{t\tau} \rangle \quad (\text{B10})$$

$v_t^{pcm}(\mathbf{r})$  represents only ligands as point charges (monopoles).

The remaining contributions are convenient to be presented as a part of the electrostatic model, which includes all ions in the crystal represented by a sequence of point monopole, dipole, quadrupole etc.:

$$V^{el} = V^{nn.pol} + V^{fn} + V^{pcm}. \quad (\text{B11})$$

Note, that the two first terms on righthanded side of Eq. (B11) are part of  $V^{res}$  in Eq. (15), whereas the third term enters into  $V^{pr}$  in Eq (13). The electrostatic potential  $V^{el}$  of point multipoles can be expanded into series of spherical harmonics, similarly as the global CF potential in Eq. (1). The corresponding contribution to the  $B_{kq}$  parameters have the following form:<sup>10</sup>

$$B_{kq}^{el} = \langle r^k \rangle \sum_t \sum_n \sum_\mu (-1)^{k+q+\mu} \left[ \frac{(2k+2n+1)!}{2^n(2k)!} \right]^{1/2} \begin{pmatrix} k & n & k+n \\ q & \mu & -q-\mu \end{pmatrix} \frac{1}{R^{k+n+1}} M_{t\mu}^{(n)} C_{q+\mu}^{(k+n)}(\mathbf{R}_t/R_t), \quad (\text{B12})$$

where  $\langle r^k \rangle$  is a mean value of  $r^k$  for the 5*f* orbital.  $\mathbf{M}_t^{(n)}$  is the 2*n*-pole electric momentum induced on ion  $t$ , where  $t$  runs over the all ions in the infinite net and  $\mu$  runs over the components of  $\mathbf{M}_t^{(n)}$ . The state of electrostatic

equilibrium between the  $\mathbf{M}_t^{(n)}$  moment and the remaining multipole moments of the crystal lattice is represented by the following equations determining the electric multipole moments  $\mathbf{M}_t^{(n)}$ :<sup>10,14</sup>

$$\mathbf{M}_t^{(n)} = \sum_{t'} \sum_{p=0,1,2} (-1)^{n+1} \alpha_t^{(n)} \mathbf{I}^{(2n)} \nabla_{t'}^{(n)} \left[ \mathbf{M}_{t'}^{(p)} \cdot \nabla_{t'}^{(p)} \frac{1}{\mathbf{R}_{t'}} \right] \quad (\text{B13})$$

where  $\mathbf{I}^{(2n)}$  is the diagonal unit tensor of rank 2*n*.  $\alpha_t^{(n)}$  is the 2*n*-pole polarizability.

### APPENDIX C:

Temperature dependence of the paramagnetic susceptibility is given by the Van Vleck formula.<sup>60</sup>

$$\chi_\alpha(T) = \frac{N_A \mu_B^2}{Z} \sum_\gamma (\beta a_{\gamma,\alpha} + 2b_{\gamma,\alpha}) \exp(-\beta E_\gamma) \quad (\text{C1})$$

with

$$a_{\gamma,\alpha} = \sum_{E_{\gamma'}=E_\gamma} |\langle \gamma | L_\alpha + gS_\alpha | \gamma' \rangle| \quad (\text{C2})$$

$$b_{\gamma,\alpha} = \sum_{E_{\gamma'} \neq E_\gamma} \frac{|\langle \gamma | L_\alpha + gS_\alpha | \gamma' \rangle|}{E_{\gamma'} - E_\gamma} \quad (\text{C3})$$

$$Z = \sum_\gamma \exp(-\beta E_\gamma) \quad (\text{C4})$$

$\beta = 1/kT$ ,  $\alpha = x, y, z$ , index  $\gamma$  numbers the eigenstates,  $E_\gamma$ 's denote their energies,  $L_\alpha$  and  $S_\alpha$  are the  $\alpha$  component of the total orbital and spin operators and  $g$  is the

gyromagnetic ratio of the electron spin.

- 
- \* e-mail: gajek@int.pan.wroc.pl
- <sup>1</sup> H. A. Bethe, Ann. Phys. (Germany) **3**, 135 (1929).
  - <sup>2</sup> C. K. Jorgensen, R. Pappalardo, and H. H. Schmidtke, J. Chem. Phys. **39**, 401 (1963).
  - <sup>3</sup> C. E. Schäffer and C. K. Jorgensen, Molecular Physics **9**, 401 (1965).
  - <sup>4</sup> M. Gerloch, J. H. Harding, and G. Wooley, Structure & Bonding **46**, 1 (1981).
  - <sup>5</sup> Z. Gajek and J. Mulak, J. Phys. : Condens. Matter **4**, 427 (1992).
  - <sup>6</sup> D. J. Newman, Adv. Phys. **20**, 197 (1971).
  - <sup>7</sup> W. Kohn and L. J. Sham, Phys. Rev. **A140**, 1133 (1965).
  - <sup>8</sup> M. Fähnle, J. Magn. Magn. Mat. **151**, L5 (1995).
  - <sup>9</sup> K. N. Kudin, G. Scuseria, and R. L. Martin, Phys. Rev. Lett. **89**, 266402 (2002), and references therein.
  - <sup>10</sup> J. Mulak and Z. Gajek, *The Effective Crystal Field Potential* (Elsevier, 2000).
  - <sup>11</sup> Z. Gajek, J. Mulak, and M. Faucher, J. Phys. Chem. Solids **48**, 947 (1987).
  - <sup>12</sup> S. Sugano and R. G. Schulman, Phys. Rev. **130**, 517 (1967).
  - <sup>13</sup> D. J. Newman and B. K. C. Ng, eds., *Crystal Field Handbook* (Cambridge, 2000).
  - <sup>14</sup> M. Faucher and D. Garcia, Phys. Rev. **B26**, 5451 (1982).
  - <sup>15</sup> P. M. Levy and S. Zhang, Phys. Rev. Lett. **62**, 78 (1989).
  - <sup>16</sup> I. A. Garifullin, T. O. Farzan, G. G. Khaliullin, and E. F. Kukovitsky, J. Phys. F: Metal Phys. **15**, 979 (1985).
  - <sup>17</sup> C. Brouder, <http://arxiv.org/list/cond-mat/0308058> (2003).
  - <sup>18</sup> D. J. Newman and B. Ng, J. Phys. C: Solid State Phys. **19**, 389 (1986).
  - <sup>19</sup> Preliminary results for  $UX_2$  have been presented at *34èmes Journées des Actinides*, Heidelberg, 17-20 April 2004.
  - <sup>20</sup> Z. Gajek, J. Phys.: Cond. Matter **12**, 415 (2000).
  - <sup>21</sup> Z. Gajek, J. Magn. Magn. Mater. **272-276**, e415 (2004).
  - <sup>22</sup> R. McWeeny and B. T. Sutcliffe, *Methods of Molecular Quantum Mechanics* (Academic Press, 1969).
  - <sup>23</sup> B. G. Wybourne, *Spectroscopic Properties of Rare Earths* (Interscience, 1965), ch. 7.
  - <sup>24</sup> C. E. Schäffer, Structure & Bonding **5**, 68 (1968).
  - <sup>25</sup> A. R. Edmonds, *Angular Momentum in Quantum Mechanics* (Princeton University Press, 1957).
  - <sup>26</sup> M. Rotenberg, R. Bivins, N. Metropolis, and J. K. Wooten, *The 3-j and 6-j Symbols* (MIT Press, 1959).
  - <sup>27</sup> M. Faucher, D. Garcia, and C. Jorgensen, Chemical Physics Letters **129**, 387 (1986).
  - <sup>28</sup> W. H. Kleiner, J. Chem. Phys. **20**, 1784 (1952).
  - <sup>29</sup> Z. Gajek and J. Mulak, Int. J. Quant. Chem. **28**, 889 (1985).
  - <sup>30</sup> N. Sato, H. Masuda, M. Wakeshima, K. Yamada, and T. J. Fujino, Alloys and Compounds **265**, 115 (1998).
  - <sup>31</sup> K. Stowe, J. Solid State Chem. **127**, 202 (1996).
  - <sup>32</sup> H. Noël, M. Potel, R. Troć, and L. Shlyk, J. Solid State Chem. **126**, 22 (1996).
  - <sup>33</sup> D. D. Koeling and B. N. Harmon, J. Phys. **C10**, 3107 (1977).
  - <sup>34</sup> D. D. Koeling (1980), Dirac-Slater atomic structure code - a derivative of the Liberman-Waber-Cromer code [Phys. Rev. **137** A27 (1965)], private communication.
  - <sup>35</sup> R. E. Watson, Phys. Rev. **111**, 1108 (1958).
  - <sup>36</sup> M. Faucher (1983), private communication.
  - <sup>37</sup> P. C. Schmidt, A. Weiss, and T. P. Das, Phys. Rev. **B19**, 5525 (1979).
  - <sup>38</sup> R. M. Sternheimer, M. Blume, and R. F. Peierls, Phys. Rev. **173**, 376 (1968).
  - <sup>39</sup> P. Erdős and J. Robinson, *The Physics of Actinide Compounds* (Plenum Press, 1983).
  - <sup>40</sup> Z. Gajek, unpublished.
  - <sup>41</sup> W. T. Carnall and H. M. Crosswhite, Tech. Rep. ANL-84/90, Argonne National Laboratory Report (1985).
  - <sup>42</sup> Z. Gajek, J. C. Krupa, and E. Antic-Fidancev, J. Phys.: Condens. Matter **6**, 557 (1997).
  - <sup>43</sup> M. Reid (1997), private communication, see also Appendix 3, p.254 in Ref. 13.
  - <sup>44</sup> Z. Gajek, M. P. Lahalle, J. C. Krupa, and J. Mulak, J. Less-Common Met. **124**, 351 (1988).
  - <sup>45</sup> R. Osborn, A. D. Taylor, Z. Bowden, M. A. Hackett, W. Hayes, M. T. Hutchings, G. Amoretti, R. Caciuffo, A. Blaise, and J. M. Furnier, J. Phys. C **21**, L931 (1988).
  - <sup>46</sup> G. Amoretti, A. Blaise, M. Bonnet, R. Caciuffo, P. Erdős, H. Noël, and P. Santini, J. Magn. Magn. Matter **139**, 339 (1995).
  - <sup>47</sup> L. Shlyk, R. Troć, and D. Kaczorowski, J. Magn. Magn. Matter **140-144**, 1435 (1995).
  - <sup>48</sup> H. Noël and R. Troć, J. Sol. St. Chem. **126**, 22 (1996).
  - <sup>49</sup> C. Rudowicz and J. Qin, J. Lumin. **110**, 39 (2004).
  - <sup>50</sup> C. Rudowicz and J. Qin, J. Alloy Compd. **385**, 238 (2004).
  - <sup>51</sup> There is no a unique set of the  $B_{kq}$  parameters in the case of low symmetry systems. Although, the parameters presented in the paper are strictly defined in the crystallographic coordination system, they have to be standardized before they are compared with other data. For further details see Refs. 10,61,62,63 and the references therein.
  - <sup>52</sup> Y. R. Shen and W. B. Holzapfel, J. Phys.: Condens. Matter **6**, 2367 (1994).
  - <sup>53</sup> Y. Shen and K. L. Bray, Phys. Rev. **B58**, 5305 (1998).
  - <sup>54</sup> G. Amoretti, A. Blaise, J. M. Collard, R. O. A. Hall, M. J. Mortimer, and R. Troć, J. Magn. Magn. Matter **46**, 57 (1984).
  - <sup>55</sup> R. Troć, Inorg. Chem. Acta **140**, 67 (1987).
  - <sup>56</sup> G. Amoretti, A. Blaise, R. Furnier, J. M. Larroque, and R. Osborn, J. Phys.: Condens. Matter **1**, 5711 (1989).
  - <sup>57</sup> R. J. Birgeneau, J. Phys. Chem. Solids **102**, 1141 (1972).
  - <sup>58</sup> Z. Gajek and J. Mulak, J. Magn. Magn. Mat. **53**, 63 (1985).
  - <sup>59</sup> G. K. Liu, *Lanthanide and actinide optical spectra*, page 65 in Ref. 13.
  - <sup>60</sup> J. H. V. Vleck, *The Theory of Electric and Magnetic Susceptibilities* (Oxford University Press, 1932).
  - <sup>61</sup> Y. Y. Yeung, *Invariants and moments*, page 160 of Ref. 13.
  - <sup>62</sup> C. Rudowicz and J. Qin, Phys. Rev. **B67**, 174420 (2003).
  - <sup>63</sup> G. W. Budrick and M. F. Reid, Mol. Phys. **33**, 59 (2004).